Original Research Paper

IJES *Iranian Journal of Earth Sciences*
*Vol. 14, No. 4, 2022, 271-284.*
DOI: 10.30495/ijes.2021.685385

# Separating geochemical anomalies by concentration- area, concentration-perimeter and concentration-number fractal models in Qaen region, East of Iran

**Mahdi Safari[1], Amir Haji Babaei[2], Ali Akbar Daya[*3], Mahya Manouchehriniya[4]**

*1. Department of Geology, Payame Noor University, Tehran, Iran*
*2. Department of Geology, Lahijan Branch, Islamic Azad University, Lahijan, Iran*
*3. Depatment of Mining Engineering, University of Sistan and Baluchestan, Zahedan, Iran.*
*4. Department of Geology, Damghan University, Damghan, Iran*

Received 11 October 2020; accepted 16 January 2021

## Abstract

The separation of geochemical anomalies from the background plays a pivotal role in geochemical exploration. Fractal and multifractal modeling of geochemical data has been recently used by numerous geoscientists. Three fractal methods were used to identify elemental geochemical anomalies in a case study from the east of the Qhaen region, southern Khorasan Province, East of Iran. These methods include concentration–area (C–A), concentration–perimeter (C–P), and concentration –number (C-N) methods. Copper mineralization occurs as vein and veinlet. Based on the analysis of heavy mineral samples, Cu contents are also observed in the southeastern, northern, and eastern parts of the Qhaen ore district, which are consistent with the results of the C–A fractal model and are genetically correlated with the andesitic unit. Indeed, after fieldwork and comparing the types of fractal models calculated, it can be concluded that the results obtained from the concentration-area method in this area were more efficient than other methods and are closer to reality.

***Keywords:*** *Concentration–area fractal model; Concentration–perimeter fractal model; concentration-number fractal model; Qhaen*

## 1. Introduction

Researchers have been employed soil geochemistry and geochemical signatures to explore minerals and also to evaluate environmental geochemistry for diverse types of deposits (e.g., Afzal et al. 2013; Hassanpour and Afzal 2013; Afzal et al. 2019; Shahsavar et al. 2020; Kouhestani et al. 2020; Saadati et al. 2020). Separating the geochemical anomalous areas from the background could be an important stage of geochemical exploration (Afzal et al. 2016). Accordingly, specimens of soil are a prevailing method that can help to demonstrate the spatial variation of the elemental concentrations (Çiftçi et al. 2005; Anand et al. 2007; Oyarzun et al. 2011; Reid and Hill, 2010; Mrvić et al. 2011). Moreover, normal or lognormal distributions describe the spreading of elements on the basis of the statistical studies (Davis 1986). The classical statistical methods could be employed by anomaly separations that have some structural features, including mean, percentile, and standard deviation (Reimann et al. 2005). However, the result of these methods cannot satisfy researchers' needs and they cannot provide a practical and real-world model, particularly for detecting weak geochemical anomalous areas, as they do not perceive spatial variance of the geochemical patterns (Davis 1986; Reimann et al. 2005; Zuo et al. 2013). After Mandelbrot (1982), fractal geometry has been utilized in various scientific fields. Likewise, Allégre and Lewin (1995) illustrated that the distribution of elements is normal or multimodal, which can be compared by fractal or multifractal models.

*Corresponding author.
*E-mail address (es):* aliakbardaya@eng.usb.ac.ir

Furthermore, freshly researchers have indicated that geochemical data can have multifractal properties (Cheng 1999, 2000, 2007; Xie and Bao 2004; Agterberg 2007; Zuo and Xia 2009; Deng et al. 2010; Pazand et al. 2011; Zuo 2011; Zuo et al. 2012; 2013; 2015; Daya 2015a; Daya 2015b; Daya and Afzal 2015; Daya et al. 2017; Aliyari et al. 2020; Ghaeminejad et al. 2020; Pourgholam et al. 2021; Yazdi et al. 2022). Currently, in order to gain a geochemical signature, researchers use fractal and multifractal models (Cheng et al. 2000; Carranza 2009; 2010) such as concentration–area (C–A), perimeter–area (P–A) (Cheng et al. 1994), concentration–distance (C–D) (Li et al. 2003), number–size (N–S) (Mandelbrot 1982; Agterberg 1995), and power spectrum–area (S–A) (Cheng et al. 1999) models. Multifractal singularity mapping in the geochemical analyses has been exclusively studied (e.g. Cheng and Agterberg 2007; Cheng 2007; Zuo and Cheng 2008; Zuo et al. 2009; Delavar et al. 2012; Yazdi et al. 2015; Naeemi et al. 2022). The concentration–perimeter (C–P) fractal model is related to the concentration–area (C–A) and perimeter–area (P–A) fractal models (Cheng 1995). In this research, the C–A, C–P, and C-N fractal methods were used to compare together as well as to understand which of these fractal methods are acceptable. Finally, for further verification of the obtained results, the distribution map of heavy mineral anomalies was also drawn.

## 2. Samples and analysis

Sampling was carried out from different rock units, as well as from stream sediments. Stream sediment samples

(n=156), 27 samples of heavy mineral, and 18 mineralized samples were collected for geochemical investigation. Stream sediment samples of the−80 mesh (0.18 mm) fraction were collected from the center of the streams. Concentrations of the elements were determined by inductively coupled plasma-mass spectrometry (ICP-MS).

International standard samples (JSD1, JSD2) and replicates were analyzed after every 10 samples for checking accuracy and precision. Mean deviations between the measured concentrations and reference values were less than 10%. Thus, the statistical parameters such as mean, average, logarithmic curves, and fractal distribution of geochemical population were calculated by Excel 10 and Arc GIS 10.1 software. The location of the stream sediment samples is shown in Figure 1.

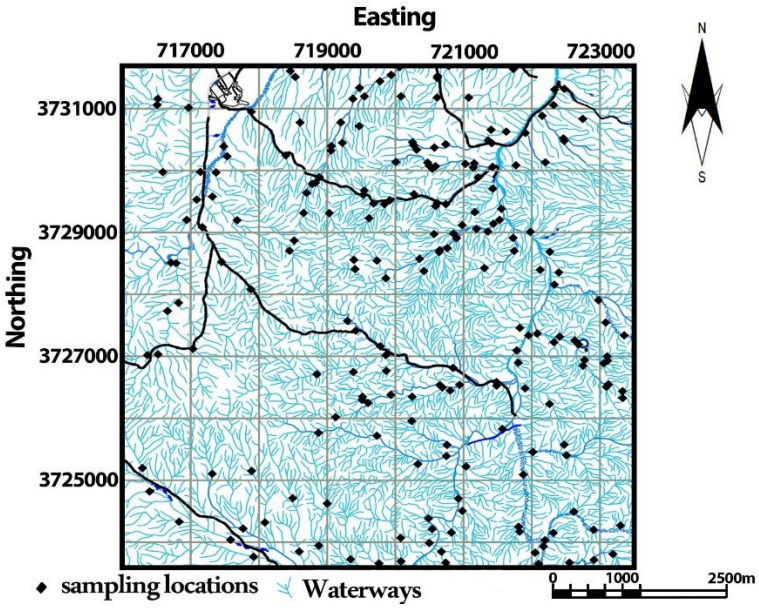


Fig 1. Location of stream sediments in east of the Qhaen area

## 3. Geological setting

The Qhaen region, with an area of 82 square kilometers, is located in the 15 km east of the Qhaen city, at a northern latitude of 33°37′ to 33°43′ and eastern longitude of 59°19′ to 59°25′, southern Khorasan Province, East of Iran. The studied area is structurally situated in the flysch zone of the East of Iran. The eastern zone of Iran is divided into two sub-zones of the Lut and the flysch zones. The eastern part of the Qhaen area has characteristics of the flysch zone, whereas its western part has characteristics of the Lut zone (Fig 2; Aghanabati 2004). The Lut block is land with an N–S trend and a length of ~900 kilometers. Its northern border is the Doruneh fault and its southern border is the Jaz Murian depression (Stöcklin et al. 1972). The main faults in the studied area have an N–S trend, whereas minor faults have NW–SE and NE–SW trends. Besides, some rock units of the studied area are separated by major faults that are strike-slip. The Upper Cretaceous limestone complex is the oldest unit in the Qhaen area, consisting of marl, siltstone, and sandstone with a light gray to greenish-gray color. The Paleocene–Eocene conglomerate in the western and southern parts of the Qhaen area was covered by the limestone. Flysches of Paleocene–Eocene are mainly made of sandstone, shale, and turbidite sediments. All of which are composed of tuffite sandstone, siltstone, argillite, marl, and gypsum.

The young terraces cover parts of low-slope and the Quaternary alluvial fans. The observed hydrothermal alterations in the studied area are mainly related to the basalt and andesitic basalt rocks. Alteration zones in the studied area are sericitic, chloritic, silicic, carbonatic, and Fe-oxyhydroxides alterations. Copper mineralization occurs as vein and veinlet and is genetically related to the basalt and andesitic basalt units (Qhasem Poor et al. 2016). Malachite, chalcocite, digenite, bornite, chalcopyrite, and covellite are the main minerals. Paleocene-Eocene magmatism in the Qhaen area caused the widespread occurrence of volcanic rocks of intermediate composition. After tectonic activities of the Middle Eocene, ore-forming fluids were deposited within the fractures and available open spaces. The different phases of faulting provided a complex network of faults in different directions. They are thrust, thrust over, and strike-slip faults.

Result of studies of the polished section and the element analysis using ICP-OES method from harvested cases from the sheets with mineralization represents this issue that the average copper grade is about 0.9%, and tungsten, molybdenum and gold respectively are about

180, 59, 0.35 g/t. The study of polished sections of the area from the sheets and silica zones shows that mineralization of chalcopyrite, pyrite, malachite, azurite, garnet and magnetite occurred. The superficial mineralization are mostly oxidized in the surface and in the study of the sections a great volume of metamorphosed sulfite minerals are seen, so that healthy chalcopyrite is seen in the form of remaining among oxides and iron hydroxides and they are dissolved to secondary minerals of chalcocite and covelite.

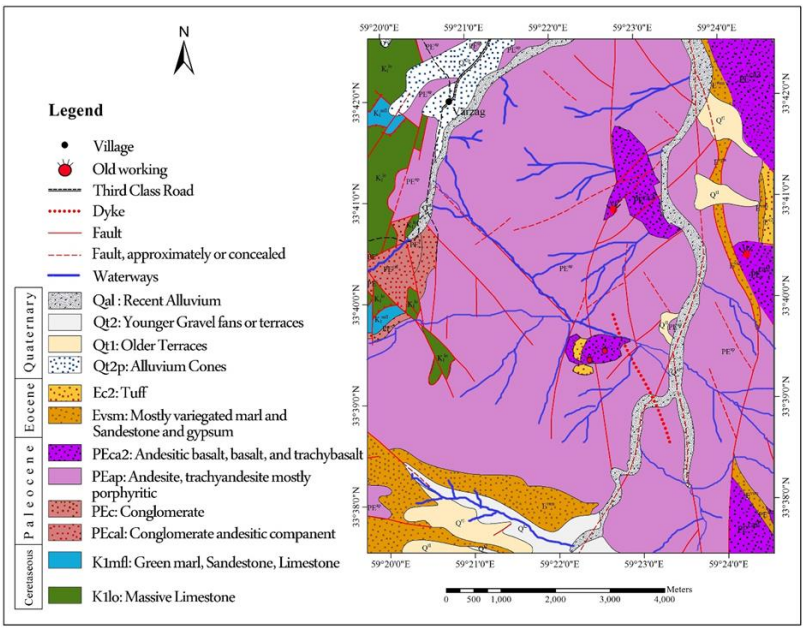


Fig 2. Geological map of east of the Qhaen area, southern Khorasan Province, East of Iran (Aghanabati 2004)

## 4. Methods

### 4. 1. Concentration–area (C–A) model

Cheng et al. (1994) suggested the concentration–area (C–A) method that has been employed to divide geochemical anomalies from the background. Concentration–area (C–A) method is as follow:

$A(\rho \leq v) \propto \rho^{-a1}$; $A(\rho \geq v) \propto \rho^{-a2}$

Where A(ρ) represents the area with concentration values greater than the contour value ρ, v depicts the threshold, and –a1 and –a2 are fractal dimensions. In this log–log plot, we have breaks between straight-line segments, and the corresponding values of ρ have been employed as thresholds to split geochemical values into various components.

### 4. 2. Concentration–perimeter (C–P) model

The C–P fractal model is as below:

$P(\rho \leq v) \propto \rho^{-a1}$; $P(\rho \geq v) \propto \rho^{-a2}$

Where P(ρ) indicates the perimeter with concentration values greater than the contour value ρ, v illustrates the threshold, –a1 and –a2 are fractal dimensions, and P(ρ) is the perimeter surrounded by the contour value ρ on a geochemical contour map resulting from the interpolation of the original data by the weighted moving average method.

### 4. 3. Concentration-Number (C-N) model

Hassanpour and Afzal (2013) suggested the concentration–number (C-N) method having applied to explain the distribution of the geochemical population. In this method, there is not any pre-processing for geochemical data (Hassanpour and Afzal, 2013). The relationship between desirable properties and their cumulative numbers of samples can be shown by this model (Sadeghi et al. 2012). A power-law frequency model has been introduced to describe the C-N method according to the frequency distribution of elemental concentrations and the cumulative number of samples with those properties (e.g., Li et al. 1994; Sanderson et al. 1994; Turcotte 1996; Shi and Wang 1998; Zuo et al. 2009; Sadeghi et al. 2012). The following equation shows the definition of the model (Mandelbrot 1983; Deng et al. 2010):

$N(\geq \rho) = K\rho^{-D}$

Where ρ indicates elemental concentration, N(≥ρ) implies the cumulative number of samples with concentration values greater than or equal to ρ, while K is constant; besides, D is the dimension of the distribution of elemental concentrations. On the basis of Mandelbrot (1983) and Deng et al. (2010), log–log plots of N(≥ρ) against ρ illustrate straight line segments with different slopes –D regarding varied concentration intervals (Sadeghi et al. 2012).

## 5. Results and discussion

Fractal geometry methods are one of the most applicable methods to study the distribution of geochemical population in geological and exploration studies. In

comparison with classical statistics, due to the fact that fractal geometry is the nature of geometry, it automatically omits off-line data and no variations in data are required. Identifying geochemical anomaly zones is one of the priorities of exploration projects. Therefore, in the study area, in addition to identifying these areas, three fractal methods include the C–A area, C–P, and N–S have been compared with each other. The mean values of Cu, Ag, Pb, and Zn in the analyzed samples are 35, 0.48, 10.3, and 61 ppm, respectively. The distribution of these elements in the analyzed samples from the Qhaen area is shown in Fig 3 and Table 1 presents the statistical parameters.

Table 1. Statistical parameters for 156 stream sediment samples from east of the Qhaen region in ppm.

| Variable | Mean | Median | St-dv | +S$\bar{X}$ | +2S$\bar{X}$ | +3S$\bar{X}$ |
|---|---|---|---|---|---|---|
| Ag | 0.48 | 0.45 | 0.15 | 0.63 | 0.78 | 0.93 |
| Cu | 35 | 33.24 | 9.8 | 44.8 | 54.6 | 64.4 |
| Pb | 10.3 | 10.25 | 1.94 | 12.24 | 14.2 | 16.15 |
| Zn | 61 | 58.7 | 11.3 | 72.3 | 83.6 | 95 |

$\bar{X}$: Mean ; S= Std.deviation

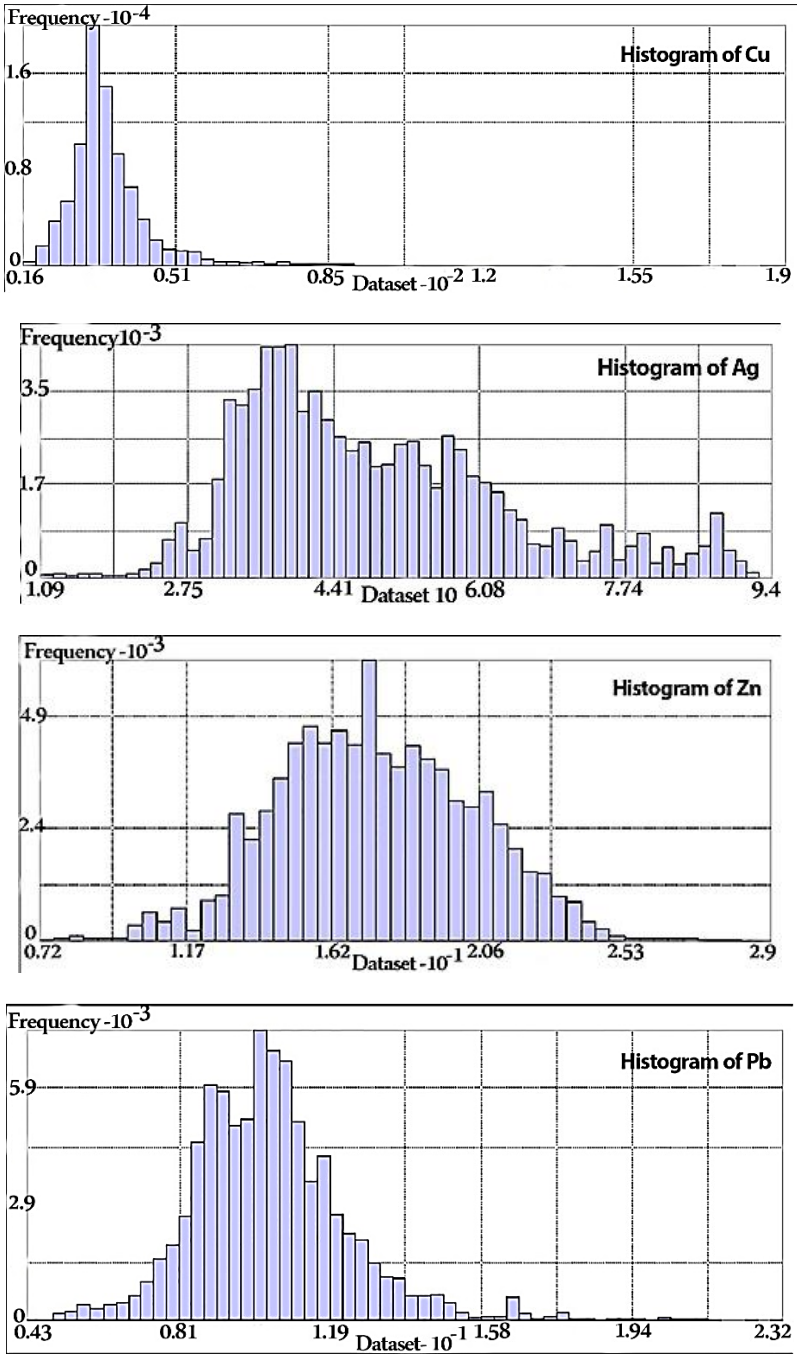


Fig 3. Histogram of Cu, Ag, Zn, and Pb for the stream sediment samples from east of the Qhaen area.

To select the best interpolation method, several factors are compared with the initial data. An optimal method is a method that generally has a higher mean value compared to the average raw data and has less variance. On the other hand, it has a meaningful relationship with its mode and median values. Therefore, the size of the samples less than the threshold remains within the logical limit. The Qhaen area was gridded by 100 m × 100 m cells, which was determined based on the geometrical properties of the studied area and sampling spacing (David 1977). In general, geostatistical estimation is a process in which one can obtain a value of a quantity at points with known coordinates using the same quantity elsewhere. Variograms and elliptical anisotropy are considered the most important components of geostatistical modeling and spatial interpolation. The variance of the elements between the points to the distance from each other can express the mutual correlation of the value of two points to the distance. In the case of a spatial structure, it is natural that the dependence of values of the points together in a deposit is greater than that of values of the distant points. This variance related to distance is called as variogram. According to the direction, the variograms are categorized into directional and omnidirectional variograms. In calculating the variogram at a given step, if the vector locates in any direction, the resulting variogram is called an omnidirectional variogram. The omnidirectional variograms and their fitted spherical models for Pb, Cu, Ag, and Zn were generated based on the data (Fig 4). As can be seen below, the graphs are plotted based on data covariance, which shows the similarity of the statistical populations in terms of distance. The radius of the impact of all elements is estimated to be about 1700-2000 meters, which is a function of Lag distance that represents the average sampling intervals. The effect of a fraction in Ag was 150, in Cu 70, in Pb, and Zn in 500 and 900, which could be due to inappropriate calibration of analyzers to chemically decompose samples containing Pb and Zn. The variogram slope is very low in all cases, which can indicate the consistency of the deposit and sampling in the region, given the large sampling intervals, tolerance, and bandwidth that give us a perfect analysis. The trend is not seen in any of the samples, but the Zn variogram shows traces of the upward trend and the degree of trend. Generally, the Cu and Zn mineralization in the studied area occurs in the andesite unit that is considered as one of the most important ore rock associated with epithermal mineralization. Interestingly, the Au contents in the analyzed samples are low.

Likewise, results of examining fitted models are presented in table 2. The grid models derived from the ordinary kriging method for Cu, Ag, Pb, and Zn that were used as inputs to Arc GIS 10.1 software, as shown in Fig 5.

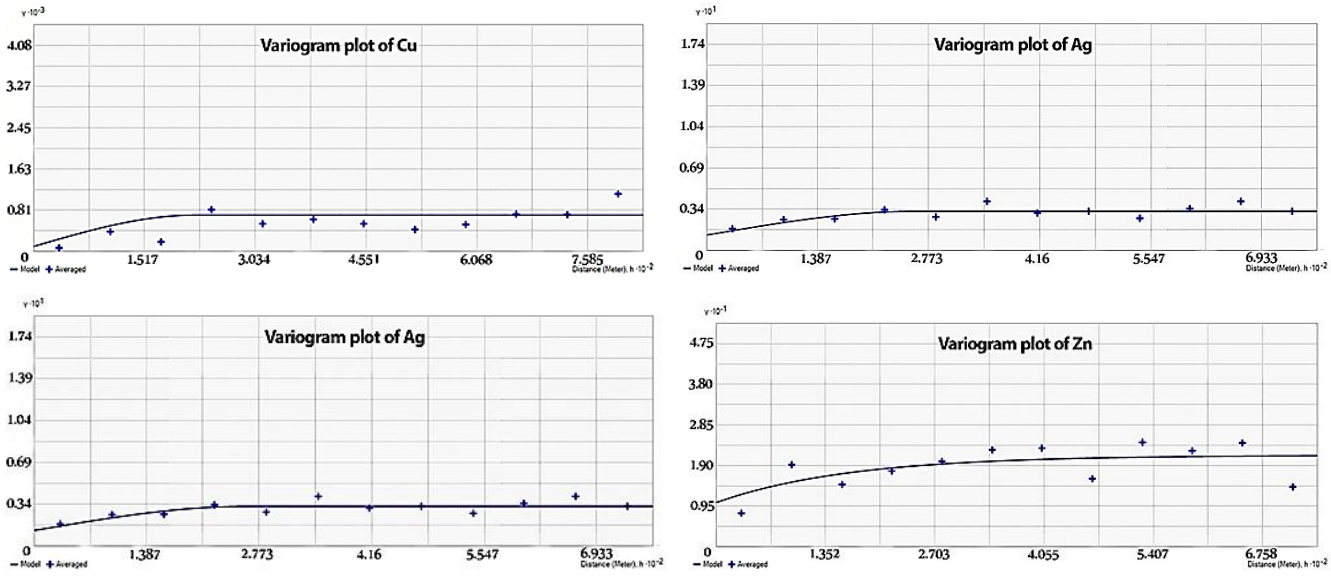


Fig 4. Variograms and fitted models for Cu, Ag, Pb, and Zn Pb in the Qhaen area.

Table 2. Results of examining fitted models.

| Variable | Model | Anisotropy | Major range | Minor range | C0 | Nugget effect |
|---|---|---|---|---|---|---|
| Ag | Spherical | × | 260 | - | 210 | 130 |
| Cu | Exponential | × | 520 | - | 250 | 120 |
| Pb | Spherical | √ | 480 | 167 | 135 | 145 |

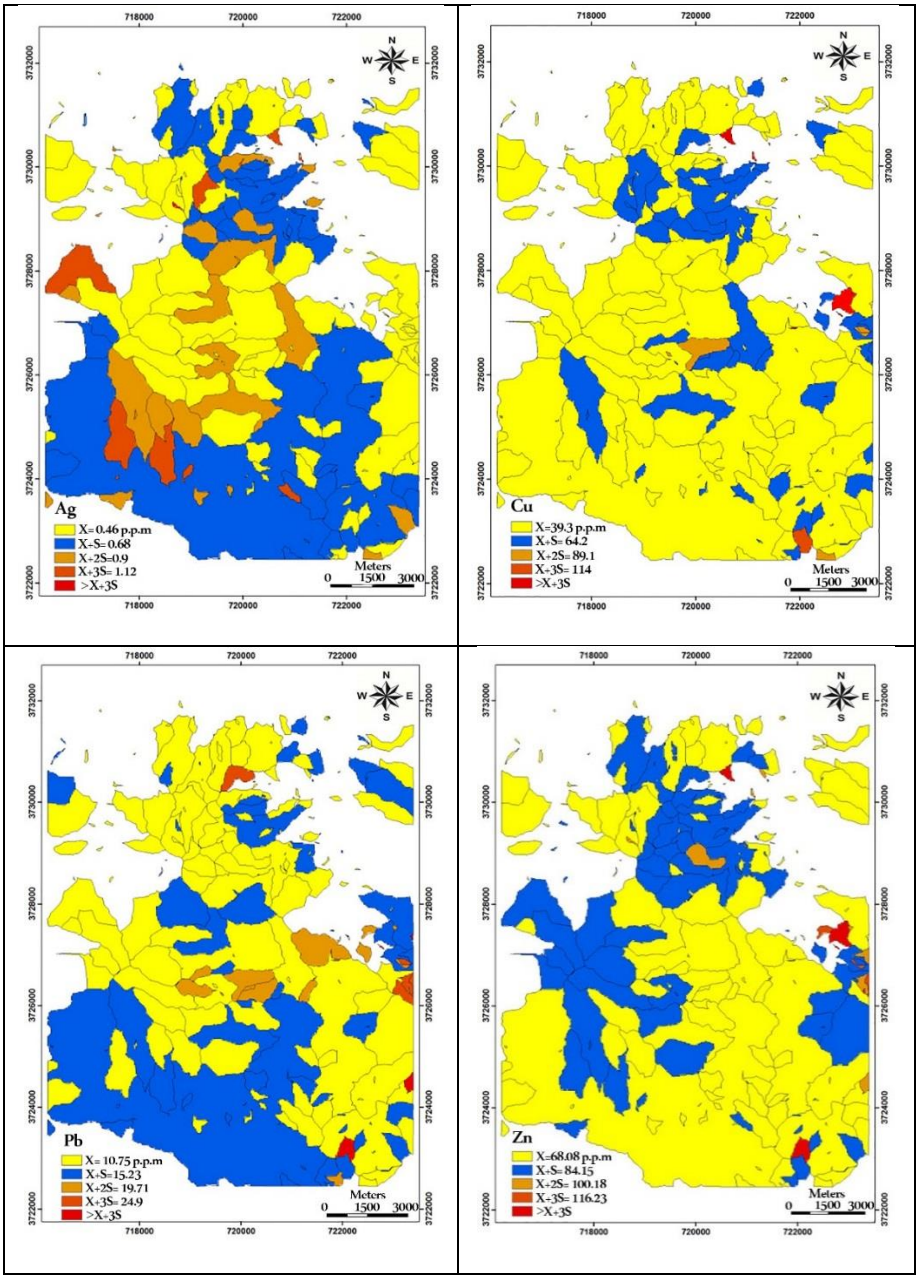


Fig 5. Distribution maps of Ag, Cu, Pb, and Zn in the Qhaen area.

C–A log–log plots for Ag, Cu, Pb, and Zn demonstrated four index breaking points and two enrichment stages (Fig 6 and Table 3). On the basis of the C–A log–log plot, the threshold value of Ag is 0.76 ppm. It means that where the threshold values are considerably in breaking points between straight-line segments, lower values are background and most of them are anomalous. The mineralization mainly occurs in grades above 0.91 ppm (Fig 6). Based on the C–A log–log plot, there are four index breaking points and two enrichment steps for Cu within the threshold values of 30 ppm and 90 ppm (Table 3). The populations higher than 65 ppm had a high enrichment step of Cu. Also, three index breaking points and two enrichment stages are observed in the logarithmic graph for Pb. Hence, the threshold value of Pb is 10.7 ppm, and mineralization mainly occurs in grades above 13.7 ppm. Their threshold values are 10.3 ppm and 21.5 ppm, as presented in Table 3. In the case of Zn, the threshold value is 69 ppm and mineralization mainly occurs in grades above 85 ppm. The C–P log–log plots for Ag, Cu, Pb, and Zn are the same as the C–A log–log plot (Fig 7). The N–S log–log plots for Ag, Cu, Pb, and Zn are shown in Fig 9. Generally, the output of Ag and Pb in the C–P and C–A log–log plots had similar characteristics. Also, for Cu and Zn, there is a similarity between the C–P and C-N outputs (Fig 7 and 8).

Table 3. Thresholds of the C–A, C–P, and C–N fractal methods for geochemical anomalies of Ag, Cu, Pb, and Zn in the Qhaen region.

| | | Ag (ppm) | Cu (ppm) | Pb (ppm) | Zn (ppm) |
|---|---|---|---|---|---|
| C–A | Low background | 0–0.53 | 0–30 | 0–10.3 | 0–69 |
| | High background | 0.53–1.03 | 30–90 | 10.3–21.5 | 69–112 |
| | Anomaly | >1.03 | >90 | >21.5 | >112 |
| C–N | Low background | 0–0.51 | 0–74 | 0–8.3 | 0–93 |
| | High background | 0.51–0.68 | 74–173 | 8.3–15.5 | 93–166 |
| | Anomaly | >0.68 | >173 | >15.5 | >166 |
| C–P | Low background | 0–0.8 | 0–85 | 0–19 | 0–91 |
| | High background | 0.8–0.95 | 85–195 | 19–24 | 91–162 |
| | Anomaly | >0.95 | >195 | >24 | >162 |

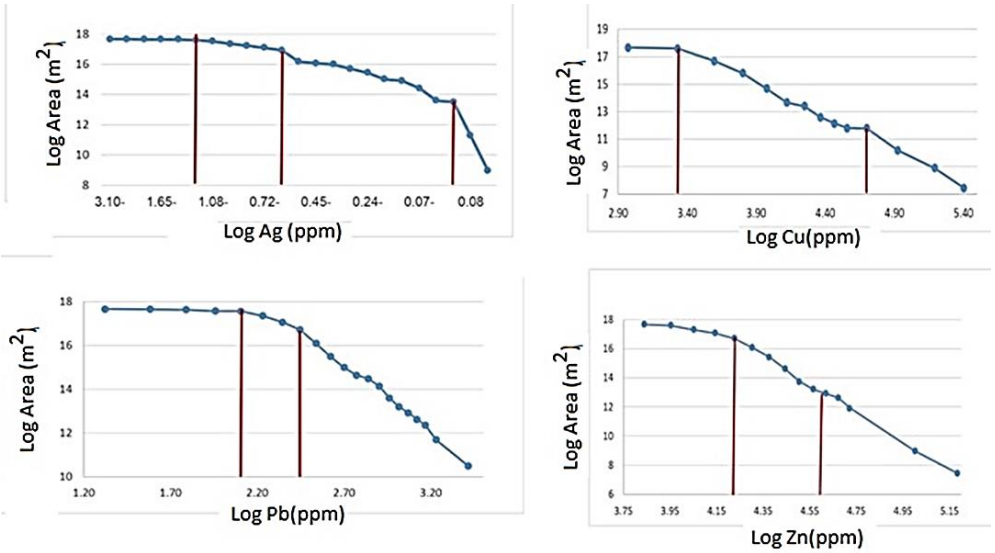


Fig 6. C–A log–log plots for Ag, Cu, Pb, and Zn in the Qhaen area.

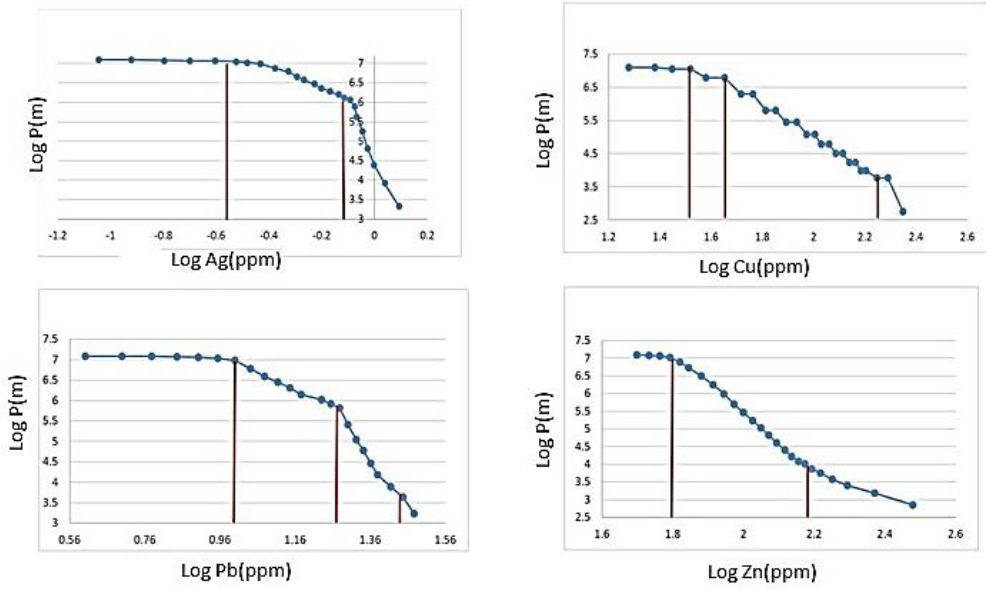


Fig 7. C–P log–log plots for Ag, Cu, Pb, and Zn in the Qhaen area.

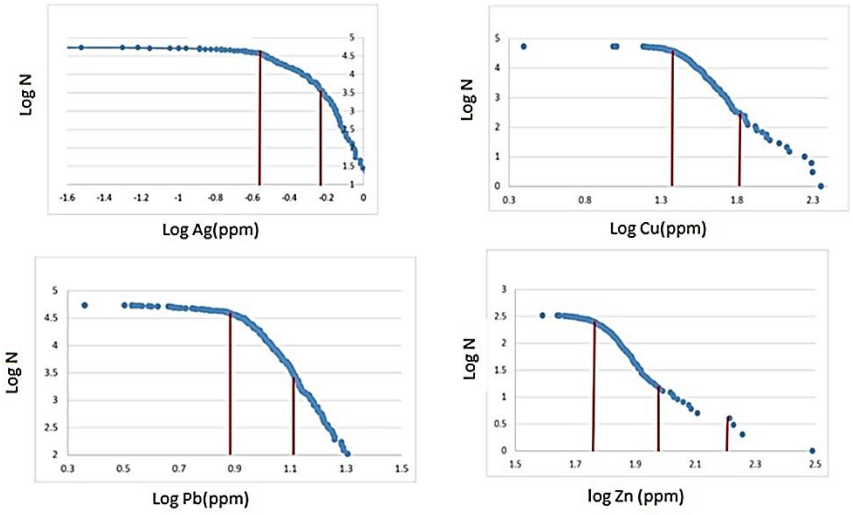


Fig 8. C-N log–log plots for Ag, Cu, Pb, and Zn in the Qhaen area.

According to C–A, C–P, and C-N methods, anomalous maps of Ag, Cu, Pb, and Zn are shown in Figs. 9–11. The anomalies observed in Ag by C–A method is located in the southwest and by C–P method is in the north and southwest, while C-N method is different from the other two methods located in the central, western, and southwestern part. (Figs. 9–11). The Cu anomaly can be seen in the north, the east, and the southeast of the areas by applying C–A, C–P, and C-N methods. (Figs. 9-11). The Pb anomaly in the C–A method is similar to the Cu anomaly.

Pb anomaly can be seen in the north, the east, and the southeast; however, there is an anomaly in the eastern in the C–P method. The C-N method shows the central and the eastern part of the area have a high anomaly of Pb (Figs. 9-11). Zn anomalies in the C–A method are very similar to those of Cu in the north, the east, and the southeast. The anomalies of Zn in C–P and C-N methods are similar together and show a weak anomaly in the eastern part (Figs. 9-11).

In order to compare the three fractal methods used for Ag, Cu, Pb, and Zn together, it is observed that in the Ag, the C-A and C-P methods are similar. In the Cu, all three methods are similar and exhibit almost identical anomalies while it is a bit different in each of the three methods in relation to Pb. Finally, the Zn element is a bit similar to the Cu anomalies in the C–A method, and the other two methods, C–P and C-N is slightly similar. In general, it can be inferred that there is little similarity between the three methods used together.

However, these similarities are slightly more pronounced in the two C–A and C–P models, especially for Cu, Ag, and Zn (Figs. 9-11).

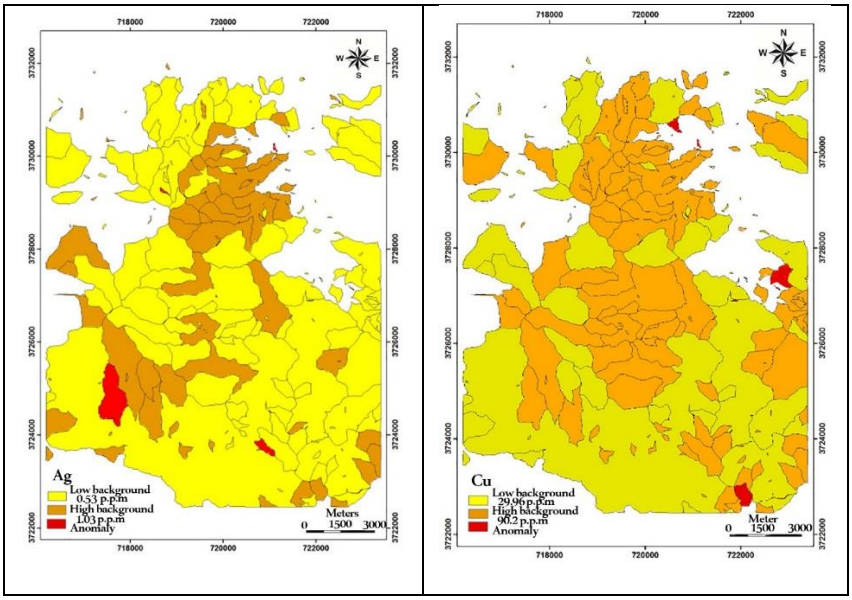


Fig 9. Ag, Cu, Pb, and Zn anomalies from the C–A plot in the Qhaen region.

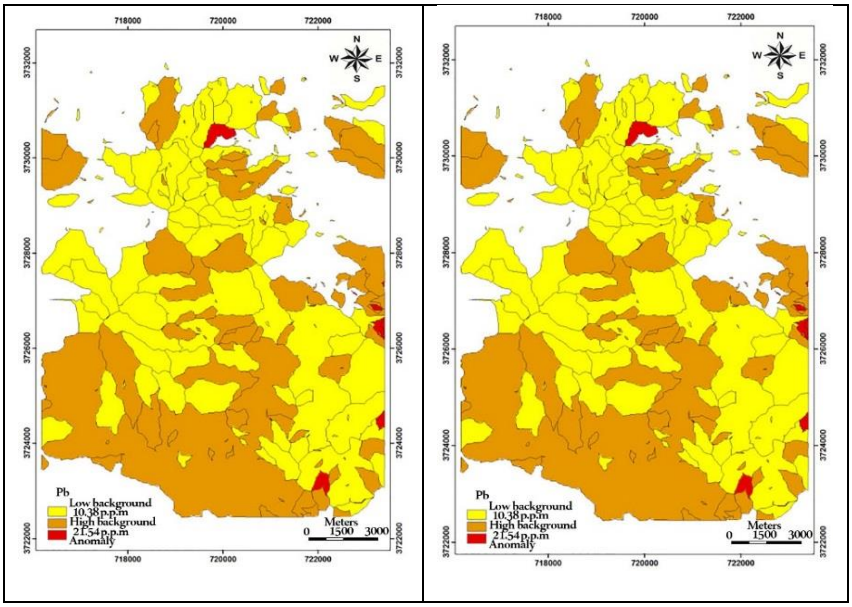


Fig 9. Continued.

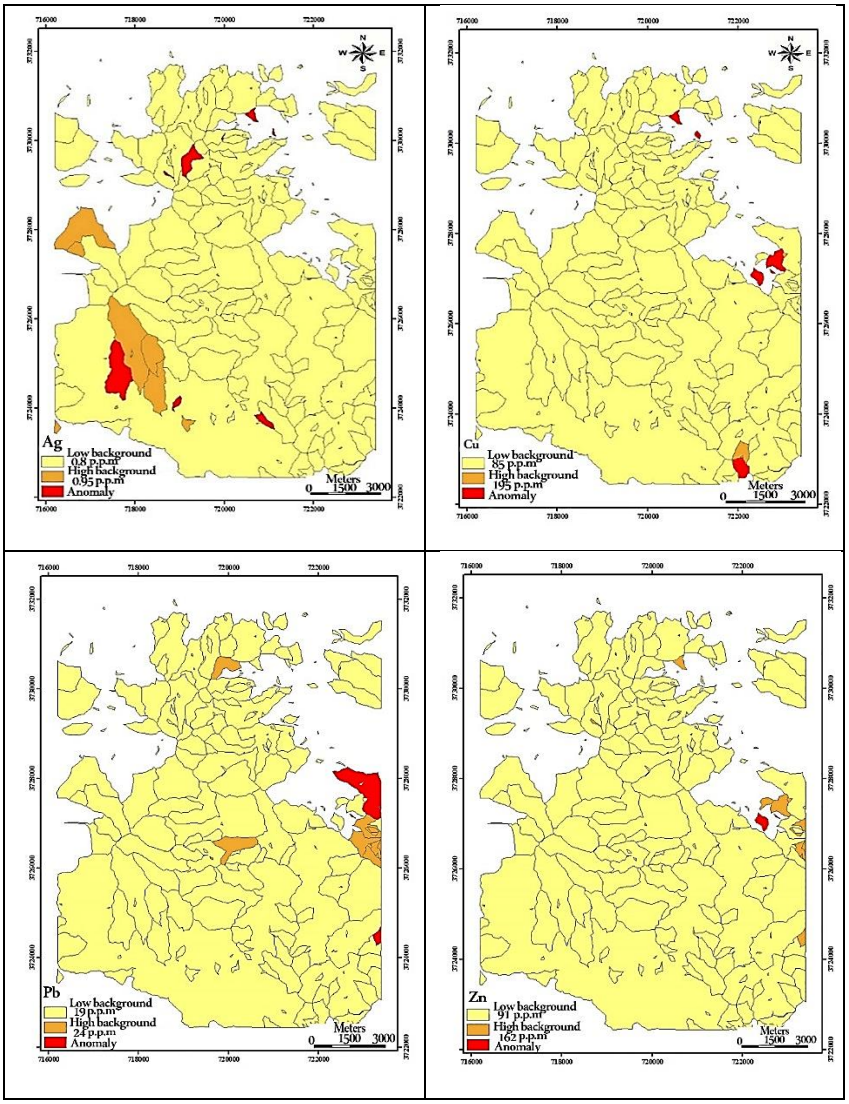


Fig 10. Ag, Cu, Pb, and Zn anomalies from the C–P plot in the Qhaen region.

The obtained threshold values from the C–A, C–P, and C-N methods were correlated with the lithological units in the Qhaen region.

High enrichment step of Ag from the C–A method is observed in the southwestern and a bit in the southern parts of the studied area, which is correlated with the andesite, marl, and sandstone units. Moderate enrichment step of Ag is also observed in the southwestern part in the andesite, marl, and sandstone units, in the central part in the andesitic unit, as well as in the western part in the conglomerate unit. In detail, based on the C–P method for Ag, there is a similarity between the southwestern part and the southern part. Although, the C–P method shows a more enrichment of Ag in the northern part of the Qhaen area in comparison with the C–A method. Based on the C-N method, the high anomaly of Ag is observed in the southwestern, western, and central parts of the studied area, which is slightly different from the resultant results of the C–A and C–P methods. Due to the fact that the thresholds of the C–A and C–P methods are similar; the Ag anomalous maps are approximately in the same shape.

High enrichment step of Cu from the C–A method is observed in the northern, southeastern, and eastern parts of the Qhaen area, which is correlated with the andesitic unit. Besides, moderate Cu anomalies are observed in the central, eastern, and northern parts. The anomalies identified for copper are similar in all three methods, but most of the C-P and C-N methods are similar.

Based on the C–A method, high concentrations of Pb are observed in the northern, southeastern, and eastern parts of the studied area, corresponding with the andesitic unit. However, based on the C–A and C-N methods, moderate Pb anomalies are widespread and they are concentrated mostly in the eastern, southern, and central parts that are correlated with tuff, andesitic basalt, basalt, andesite, marl, and sandstone.

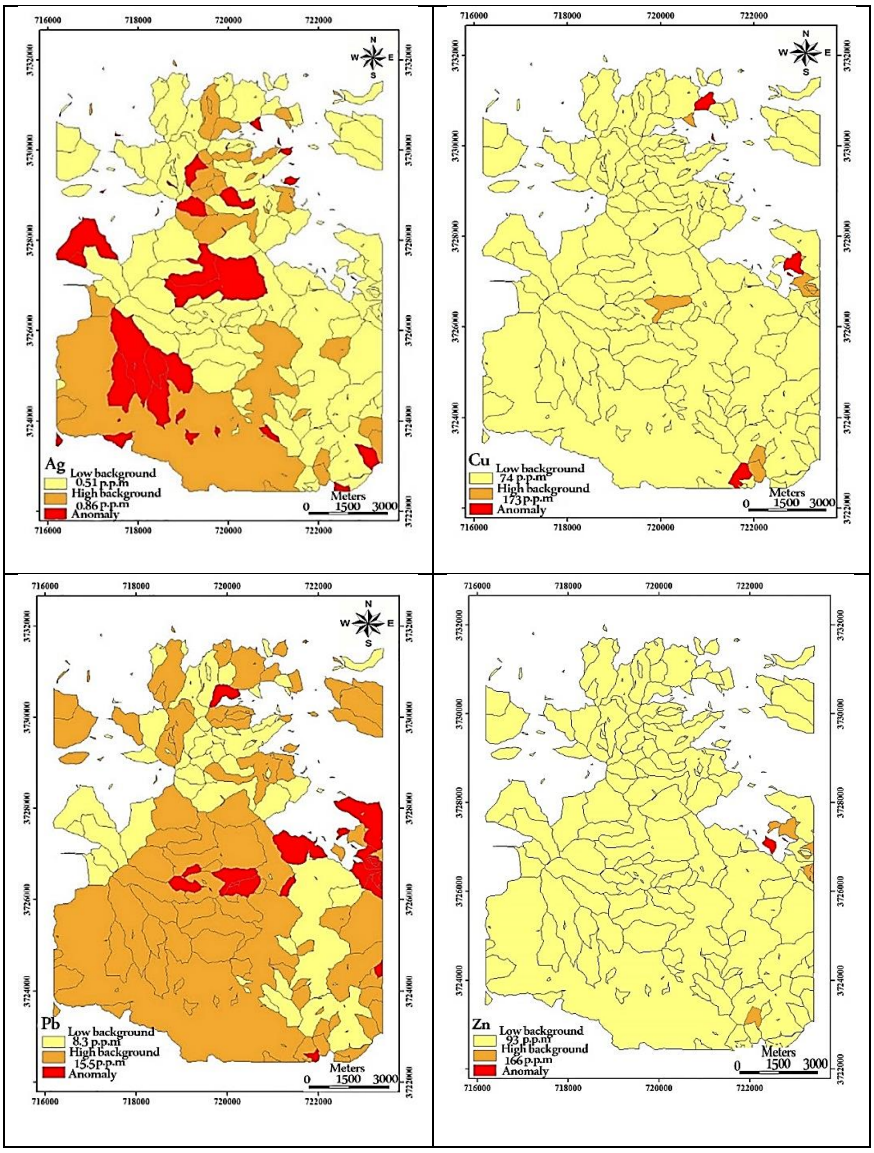


Fig 11. Ag, Cu, Pb, and Zn anomalies from the C-N plot in the Qhaen region.

Zn also indicates an anomaly that is similar to Cu in the C–A method, showing anomalies in the north, the east, and the southeast, these anomalies are correlated by the andesitic unit of the studied area. In addition, the moderate anomaly of Zn is also in the northern, central and eastern parts of the studied area is very similar to the Cu. In the C–P method, a very small anomaly is shown in the eastern part and a large moderate anomaly is not detectable. A weak moderate anomaly can be observed in the east of the area. In detail, there is a positive relationship between Cu and Zn anomalous areas especially in the C-A method in the northern, southeastern, and eastern parts of the Qhaen area that make them worthy of further investigation. However, Au and Ag values in the analyzed samples are low.

As mentioned above, the main faults in the Qhaen area have an N-S trend, whereas minor faults have NW–SE and NE–SW trends. Most of the faults in the region are well correlated to Cu, Pb, and Zn mineralization. The dyke observed in the study area is also in the north-south trend, which almost follows the main faults of the study area. No alteration or mineralization zones have been observed around this dyke, which may indicate that the dyke is unrelated to mineralization in the area. Fig 12 shows the distribution maps of Cu and Fe, based on 27 heavy mineral samples (Table. 4). The highest enrichment step of Cu occurs in the southeastern, northern, and eastern parts of the studied area (Fig 12), which is consistent with the results of the C–A fractal model.

There also is anomalies of Fe-oxyhydroxides in the southeastern part of the Qhaen area. Indeed, after field studies, and the comparison of the types of fractal models made, it can be concluded that the results obtained from the concentration-area method in this area were more efficient than other methods and are closer to reality.

Table 4. Results of Cu, Pb, and Zn anomalies of 27 heavy mineral samples from the Qhaen area.

| Name anomaly | Heavy mineral | Rock type | Zn (ppm) | Cu (ppm) | Pb (ppm) |
|---|---|---|---|---|---|
| Cu | LV-03 | Andesite | 2.03 | 1340 | 17 |
| | LV-04 | Andesite | 12.9 | 3450 | 61 |
| | LV-05 | Andesite | 36.1 | 4240 | 78 |
| Pb | LV-06 | Turbidity | 23 | 2970 | 847 |
| | LV-08 | Andesite | 14 | 2570 | 209 |
| | LV-10 | Conglomerate and tuff | 3 | 8900 | 55 |
| Zn | LV-01 | Andesite | 9.38 | 2100 | 45 |
| | LV-02 | Andesite | 31 | 4240 | 78 |

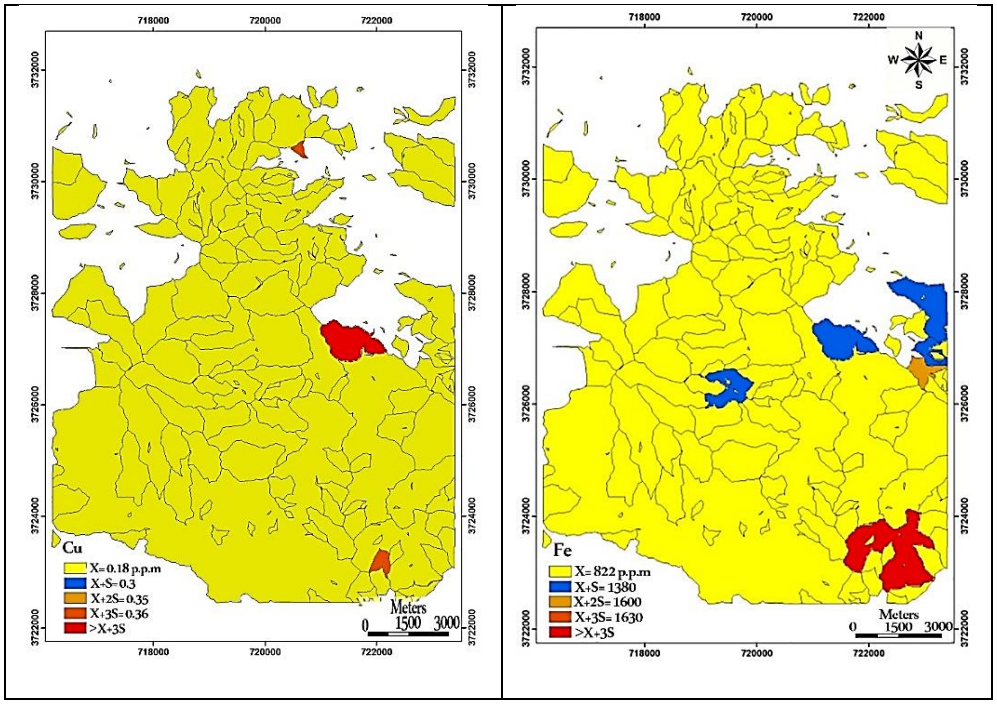


Fig 12. Distribution maps of Cu and Fe-oxyhydroxides from heavy minerals from the Qhaen area.

## 6. Conclusions

Malachite, chalcocite, digenite, bornite, chalcopyrite, and, covellite are the main minerals in the Qhaen area. Chalcopyrite and magnetite, as the primary minerals, were converted to covellite, malachite, chalcocite, and limonite. Copper mineralization occurs mainly as vein and veinlet that is genetically related to the andesitic rocks.

Undoubtedly, fractal geometry methods are one of the best and most applicable methods for studying the distribution of geochemical populations in geological and exploration studies. In comparison with classical statistics, it automatically deletes off-line data, and no change in data is required due to the fact that fractal geometry is the nature of geometry. The bivariate statistical studies have shown the accuracy and precision of the C–A method.

Based on the Cu and Zn anomalies maps, the suggested anomalous areas identified by the C–P and C-N methods were approximately similar. According to the maps of Ag, Cu, Pb, and Zn geochemical anomalies, the suggested anomalous areas identified by the C–A and C–P models were approximately in the same shape and location. The Cu anomaly is similar in all three methods and indicates almost identical anomalies. In the Pb, the similarities are very small in all three methods. Finally, the Zn is a bit similar to the Cu anomalies in the C–A method, and in other two methods, C–P and C-N, are slightly similar. In general, it can be inferred that there is a little similarity among the three methods used. However, these similarities are slightly more pronounced in the two C–A and C–P models, especially related to Cu, Ag, and Zn. Based on the analysis of heavy mineral samples, anomalies of Cu are also seen in the southeastern, northern, and eastern parts of the studied area, consistent with obtained results of the C–A fractal model. Indeed, after fieldwork, extracted quarries, and comparing the types of fractal models calculated, it can be concluded that the results obtained from the concentration-area method in this area were more efficient than other methods and are closer to reality.

## References

Afzal P, Harati H, Alghalandis YF, Yasrebi AB (2013) Application of spectrum–area fractal model to identify of geochemical anomalies based on soil data in Kahang porphyry-type Cu deposit, Iran. *Geochemistry* 73(4): 533-543.

Afzal P, Mirzaei M, Yousefi M, Adib A, Khalajmasoumi M, Zarifi AZ, Yasrebi AB (2016) Delineation of geochemical anomalies based on stream sediment data utilizing fractal modeling and staged factor analysis. *Journal of African Earth Sciences* 119: 139-149.

Afzal P, Yousefi M, Mirzaei M, Ghadiri-Sufi E, Ghasemzadeh S, Daneshvar Saein L (2019) Delineation of podiform-type chromite mineralization using Geochemical Mineralization Prospectivity Index (GMPI) and staged factor analysis in Balvard area (southern Iran). *Journal of Mining and Environment* 10: 705-715.

Aghanabati A (2004) Geology of Iran. Geological survey of Iran.

Agterberg FP (1995) Multifractal modeling of the sizes and grades of giant and supergiant deposits. *International Geology Review*, 37(1):1-8.

Agterberg FP (2007). Mixtures of multiplicative cascade models in geochemistry.

Aliyari F, Afzal P, Lotfi M, Shokri S, Feizi H (2020) Delineation of geochemical haloes using the developed zonality index using multivariate and fractal analysis in the Cu-Mo porphyry deposits. *Applied Geochemistry* 121: 104694.

Allegre CJ, Lewin E (1995) Scaling laws and geochemical distributions. *Earth and Planetary Science Letters* 132(1-4):1-13.

Anand R R, Cornelius M, Phang C (2007) Use of vegetation and soil in mineral exploration in areas of transported overburden, Yilgarn Craton, Western Australia: a contribution towards understanding metal transportation processes. *Geochemistry: Exploration, Environment, Analysis* 7(3): 267-288.

Carranza EJ M (2010) Mapping of anomalies in continuous and discrete fields of stream sediment geochemical landscapes. *Geochemistry: Exploration, Environment, Analysis* 10(2): 171-187.

Carranza EJM (2010) Catchment basin modelling of stream sediment anomalies revisited: incorporation of EDA and fractal analysis. *Geochemistry: Exploration, Environment, Analysis* 10(4): 365-381.

Carranza EJM, Zuo R, Cheng Q (2012) Fractal/multifractal modelling of geochemical exploration data. *Journal of Geochemical Exploration* 122: 1-3.

Cheng Q (1999) Spatial and scaling modelling for geochemical anomaly separation. *Journal of Geochemical exploration* 65(3): 175-194.

Cheng Q (2007) Mapping singularities with stream sediment geochemical data for prediction of undiscovered mineral deposits in Gejiu, Yunnan Province, China. *Ore Geology Reviews* 32(1-2): 314-324.

Cheng Q, Agterberg FP (2009) Singularity analysis of ore-mineral and toxic trace elements in stream sediments. *Computers Geosciences* 35(2): 234-244.

Cheng Q, Agterberg FP, Ballantyne SB (1994) The separation of geochemical anomalies from background by fractal methods. *Journal of Geochemical Exploration* 51(2): 109-130.

Cheng, QM (2000) Multifractal Theory and Geochemical Element Distribution Pattern. *Earth Science–Journal of China University of Geosciences* 25(3): 311–318 (in Chinese with English Abstract)

Çiftçi E, Kolayli H, Tokel S (2005) Lead-arsenic soil geochemical study as an exploration guide over the Killik volcanogenic massive sulfide deposit,

Northeastern Turkey. *Journal of Geochemical Exploration* 86(1): 49-59.

David M (1977) Geostatistical ore reserve estimation: Elsevier sci. Publ Co, New York.

Davis JC, Sampson R J (1986) Statistics and data analysis in geology (Vol. 646). New York: *Wiley.*

Daya AA (2015) Comparative study of C–A, C–P, and C-N fractal methods for separating geochemical anomalies from background: A case study of Kamoshgaran region, northwest of Iran. Journal of *Geochemical Exploration* 150: 52-63.

Daya AA (2015b) Application of concentration–area method for separating geochemical anomalies from background: a case study of Shorabhaji region, northwest of Iran. *Arabian journal of geosciences*. 8:3905–3913.

Daya AA, Afzal P (2015) Comparative study of concentration-area (C-A) and spectrum-area (S-A) fractal models for separating geochemical anomalies in Shorabhaji region, NW Iran. *Arabian journal of geosciences* 8:8263–8275.

Daya AA, Boomeri M, Mazraee N (2017) Identification of Geochemical Anomalies by Using of Concentration-Area (C-A) Fractal Model in Nakhilab Region, SE Iran. *Journal of mining and mineral engineering*. 8: 70-81.

Delavar ST, Afzal P, Borg G, Rasa I, Lotfi M, Omran N R (2012) Delineation of mineralization zones using concentration–volume fractal method in Pb–Zn carbonate hosted deposits. *Journal of Geochemical Exploration* 118: 98-110.

Deng J, Wang Q, Yang L, Wang Y, Gong Q, Liu H (2010) Delineation and explanation of geochemical anomalies using fractal models in the Heqing area, Yunnan Province, China. *Journal of Geochemical Exploration* 105(3): 95-105.

Ghaeminejad H, Abedi M, Afzal P, Zaynali F, Yousefi M (2020) A fractal-based outranking approach for mineral prospectivity analysis. Bollettino di Geofisica Teorica e Applicata 61(4): 555-588.

Ghasempoor F (2016) Structural controllers on copper mineralization in the Varzg area (East of Qain-Birjand). Master's Thesis (in Persian).

Hassanpour Sh, Afzal P (2013) Application of concentration-number (C-N) multifractal modelling for geochemical anomaly separation in Haftcheshmeh porphyry system, NW Iran. *Arabian Journal of Geosciences* 6: 957–970.

Kouhestani H, Ghaderi M, Afzal P, Zaw K (2020) Classification of pyrite types using fractal and stepwise factor analyses in the Chah Zard gold-silver epithermal deposit, central Iran. Geochemistry: *Exploration, Environment, Analysis* 20 : 496-508.

Li C, Ma T, Shi J (2003) Application of a fractal method relating concentrations and distances for separation of geochemical anomalies from background. *Journal of Geochemical Exploration* 77(2-3): 167-175.

Mandelbrot B B (1982) The Fractal Geometry of. Nature, 394-397.

Mrvić V, Kostić-Kravljanac L, Čakmak D, Sikirić B, Brebanović B, Perović V, Nikoloski M (2011) Pedogeochemical mapping and background limit of trace elements in soils of Branicevo Province (Serbia). *Journal of Geochemical Exploration* 109(1-3): 18-25.

Naeemi S, Arian MA, Kohansal-Ghadimvand N, Yazdi A, Abedzadeh H (2022) Diagenesis and Tectonic Setting of the Varcheh Intrusive Masses in Sanandaj-Sirjan Zone, Iran, *Revista Geoaraguaia* 12 (1): 52-72

Oyarzun R, Lillo J, López-García J A, Esbrí J M, Cubas P, Llanos W, Higueras P (2011) The Mazarrón Pb–(Ag)–Zn mining district (SE Spain) as a source of heavy metal contamination in a semiarid realm: geochemical data from mine wastes, soils, and stream sediments. *Journal of Geochemical Exploration* 109(1-3): 113-124.

Pazand K, Hezarkhani A, Ataei M, Ghanbari Y (2011) Application of multifractal modeling technique in systematic geochemical stream sediment survey to identify copper anomalies: a case study from Ahar, Azarbaijan, Northwest Iran. *Geochemistry* 71(4): 397-402.

Pourgholam MM, Afzal P, Yasrebi AB, Gholinejad M, Wetherelt A (2021) Detection of geochemical anomalies using a fractal-wavelet model in Ipack area, Central Iran. *Journal of Geochemical Exploration* 220: 106675.

Reid N, Hill SM (2010) Biogeochemical sampling for mineral exploration in arid terrains: Tanami Gold Province, Australia. *Journal of Geochemical Exploration* 104(3): 105-117.

Reimann C, Filzmoser P, Garrett R G (2005) Background and threshold: critical comparison of methods of determination. *Science of the total environment* 346 (1-3): 1-16.

Saadati H, Afzal P, Torshian H, Solgi A (2020) Geochemical exploration for Li using Geochemical Mapping Prospectivity Index (GMPI), fractal and Stage Factor Analysis (SFA) in NE Iran. *Geochemistry: Exploration, Environment, Analysis* 20: 461-472.

Sadeghi B, Moarefvand P, Afzal P, Yasrebi A B, Saein L D (2012) Application of fractal models to outline mineralized zones in the Zaghia iron ore deposit, Central Iran. *Journal of Geochemical Exploration*: 122, 9-19.

Sanderson D J, Roberts S, Gumiel P (1994) A fractal relationship between vein thickness and gold grade in drill core from La Codosera, Spain. *Economic Geology* 89(1):168-173.

Shahsavar S, Jafari Rad AR, Afzal P, Nezafati N (2020). Selection of Optimum Fractal Model for Detection of Stream Sediments Anomalies. Geopersia 10, 395-404.

Shi J, Wang C (1998) Fractal analysis of gold deposits in China: implication for giant deposit exploration. *Earth Sci. J. China Univ. Geosci* 23: 616-618.

Stöcklin J, Ruttner A, Nabavi M H (1972) New data on the lower Paleozoic and pre-Cambrian of north Iran (No. 1). Geological Survey of Iran.

Turcotte D L (1996) Fractals and Chaos in Geophysics (pp. 81–99).

Xie S, Bao Z (2004) Fractal and multifractal properties of geochemical fields. *Mathematical Geology* 36(7): 847-864.

Yazdi A, Shahhosseini E, Moharami F (2022) Petrology and tectono-magmatic environment of the volcanic rocks of West Torud–Iran, *Iranian Journal of Earth Sciences* 14 (1): 40-57.

Yazdi A, Ziaaldini S, Dabiri R (2015) Investigation on the Geochemical Distribution of REE and Heavy Metals in Western Part of Jalal-Abad Iron Ore Deposit, Zarand, SE of Iran, *Open journal of ecology* 5 (09): 460-476.

Zuo R (2011) Identifying geochemical anomalies associated with Cu and Pb–Zn skarn mineralization using principal component analysis and spectrum–area fractal modeling in the Gangdese Belt, Tibet (China). *Journal of Geochemical Exploration*, 111(1-2), 13-22.

Zuo R, Cheng Q (2008) Mapping singularities—a technique to identify potential Cu mineral deposits using sediment geochemical data, an example for Tibet, west China. *Mineralogical Magazine* 72(1): 531-534.

Zuo R, Cheng Q, Agterberg F P, Xia Q (2009) Application of singularity mapping technique to identify local anomalies using stream sediment geochemical data, a case study from Gangdese, Tibet, western China. *Journal of Geochemical Exploration* 101(3): 225-235.

Zuo R, Wang J, Chen G, Yang M (2015) Identification of weak anomalies: A multifractal perspective. *Journal of Geochemical Exploration* 148: 12-24.

Zuo R, Xia Q (2009) Application fractal and multifractal methods to mapping prospectivity for metamorphosed sedimentary iron deposits using stream sediment geochemical data in eastern Hebei province, *China*. *GeCAS* 73: A1540.

Zuo R, Xia Q (2009) Application fractal and multifractal methods to mapping prospectivity for metamorphosed sedimentary iron deposits using stream sediment geochemical data in eastern Hebei province, *China*. *GeCAS*, 73: A1540.

Zuo R, Xia Q, Wang H (2013) Compositional data analysis in the study of integrated geochemical anomalies associated with mineralization. *Applied geochemistry* 28: 202-211.